ARMY RESEARCH LABORATORY

High Temperature Thermoelectric Materials for Waste Heat Regeneration

by Horacio Nochetto, Patrick Taylor, and Jay R. Maddux

ARL-TR-6311 **January 2013**

NOTICES

Disclaimers

The findings in this report are not to be construed as an official Department of the Army position unless so designated by other authorized documents.

Citation of manufacturer's or trade names does not constitute an official endorsement or approval of the use thereof.

Destroy this report when it is no longer needed. Do not return it to the originator.

Army Research Laboratory
Adelphi, MD 20783-1197

ARL-TR-6311 **January 2013**

High Temperature Thermoelectric Materials for Waste Heat Regeneration

Horacio Nochetto and Jay R. Maddux
General Technical Services, LLC, Wall, NJ

and

Patrick Taylor
Sensors and Electron Devices Directorate, ARL

REPORT DOCUMENTATION PAGE	Form Approved OMB No. 0704-0188

PLEASE DO NOT RETURN YOUR FORM TO THE ABOVE ADDRESS.

1. REPORT DATE *(DD-MM-YYYY)*	2. REPORT TYPE	3. DATES COVERED (From - To)
January 2013	Final	

4. TITLE AND SUBTITLE

High Temperature Thermoelectric Materials for Waste Heat Regeneration

5a. CONTRACT NUMBER

5b. GRANT NUMBER

5c. PROGRAM ELEMENT NUMBER

6. AUTHOR(S)

Horacio Nochetto, Patrick Taylor, and Jay R. Maddux

5d. PROJECT NUMBER

5e. TASK NUMBER

5f. WORK UNIT NUMBER

7. PERFORMING ORGANIZATION NAME(S) AND ADDRESS(ES)

U.S. Army Research Laboratory
ATTN: RDRL-SED-E
2800 Powder Mill Road
Adelphi, MD 20783-1197

8. PERFORMING ORGANIZATION REPORT NUMBER

ARL-TR-6311

9. SPONSORING/MONITORING AGENCY NAME(S) AND ADDRESS(ES)

10. SPONSOR/MONITOR'S ACRONYM(S)

11. SPONSOR/MONITOR'S REPORT NUMBER(S)

12. DISTRIBUTION/AVAILABILITY STATEMENT

Approved for public release; distribution unlimited.

13. SUPPLEMENTARY NOTES

14. ABSTRACT

Motivated by non-renewable petroleum consumption and the perceived climate change due to carbon dioxide (CO_2) and other greenhouse gases, effort has been focused on recuperating lost energy from hot exhaust gases. Automobiles using thermoelectric generators (TEGs) are possible solutions due to the potential for high regenerative rates associated with the amount of waste heat and the corresponding high temperature. TEGs are solid-state heat engines that contain no moving parts, and are compact, silent, and extremely scalable. This brief review covers basic thermoelectric material principles, discusses the performance of several candidate thermoelectric materials, and concludes with reliability concerns exacerbated by the high temperatures associated with automotive exhaust.

15. SUBJECT TERMS

Thermoelectric Power Generator, Thermoelectric figure-of-merit (Z or ZT), Waste Heat Recovery, Seebeck Coefficient, Reliability,

16. SECURITY CLASSIFICATION OF:			17. LIMITATION OF ABSTRACT	18. NUMBER OF PAGES	19a. NAME OF RESPONSIBLE PERSON
a. REPORT	b. ABSTRACT	c. THIS PAGE			Horacio Nochetto
Unclassified	Unclassified	Unclassified	UU	32	19b. TELEPHONE NUMBER (*Include area code*) (301) 394-2293

Standard Form 298 (Rev. 8/98)
Prescribed by ANSI Std. Z39.18

Contents

List of Figures

List of Tables

INTENTIONALLY LEFT BLANK.

1. Introduction

World energy consumption is currently increasing at a dramatic rate and it is projected that all current oil deposits will be consumed within the next 40 years if current consumption remains constant (*1*). Furthermore, this rate is expected to increase as shown in figure 1, causing the power generation, industrial, and transport industries to release elevated carbon dioxide (CO_2) emissions (*1, 2*). These environmental issues have caused a surge of renewable energy research, producing such technologies as solar (photovoltaic and solar heating), geothermal, biomass, and wind energy production. Unfortunately, these still-developing technologies are currently incapable of replacing the world's petroleum based infrastructures (*1*). Consequently, the majority of the world still heavily relies on petroleum products.

For example, the U.S. Department of Defense (DoD) alone consumes more than 3 x 10^5 barrels per day at the "fully burdened cost" of $42 per gallon due to the added costs of procurement, shipping, protection, and delivery (*3, 4*). These monetary costs are negligible in comparison to the average human cost of 1 casualty every 24 logistical supply trips (*4, 5*).

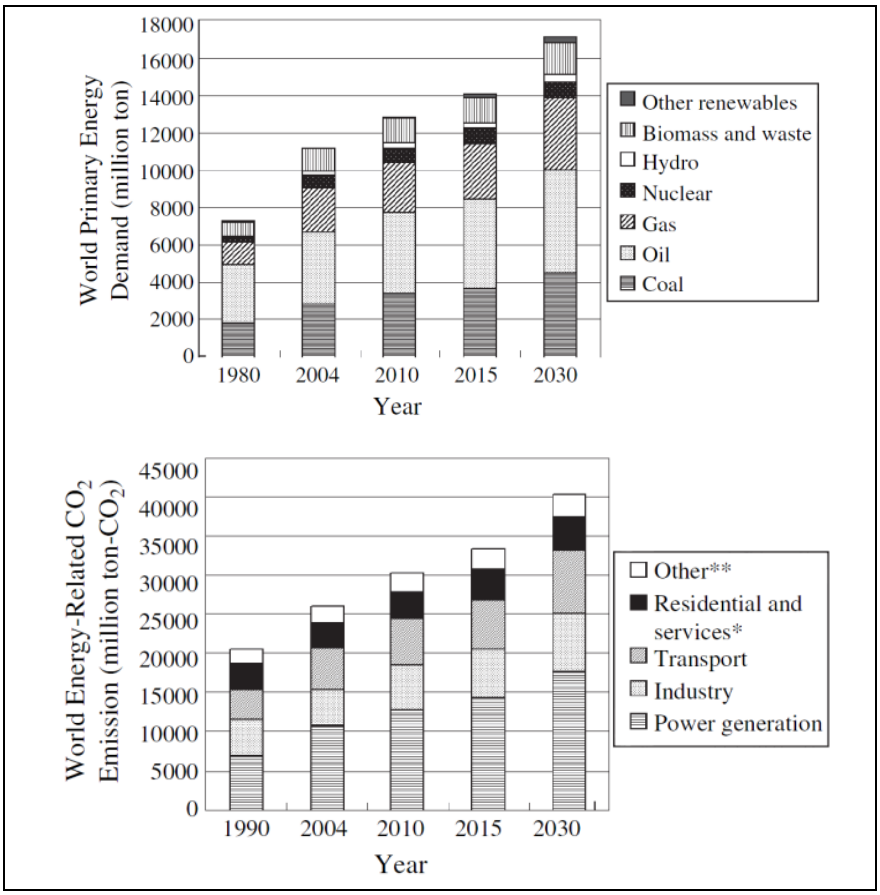

Figure 1. World energy demand and related carbon dioxide emissions (*1, 2*).

Fuel costs are so high due to the large demand required by today's inefficient infrastructures. For instance, the infrastructure in Japan only used 30% of its fuel energy for mechanical work, with the rest ejected into the atmosphere as waste heat (*1*). This waste heat, as shown in figure 2a, was categorized as a function of temperature. Automobiles clearly released much waste heat, but their losses detailed in figure 2b show the exhaust contains the largest amount of energy even when including the mobility path. This, coupled with the exhaust gases' high temperature, makes it an excellent opportunity for waste-heat recovery technologies.

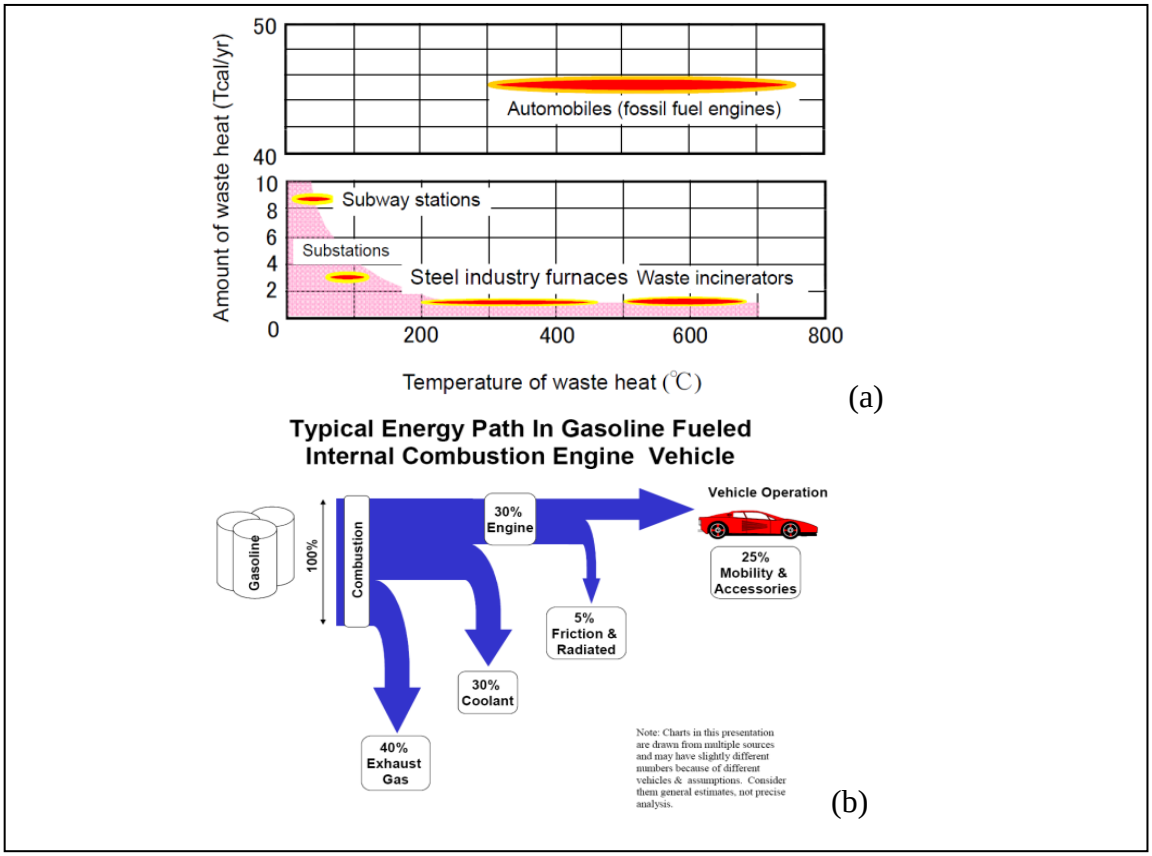

Figure 2. (a) Annual amount of waste heat as a function of temperature for Japan (*26*, *19*). (b) Energy path in a gasoline powered automobile (*27*, *28*).

Thermoelectric (TE) generators (TEGs) offer a viable solution to high temperature waste heat regeneration since they are solid-state heat engines with no moving parts, and are compact, silent, and scalable (*6*). As shown by table 1, the National Aeronautics and Space Administration's (NASA) deep space explorations, which use radioisotope thermoelectric generators (RTGs) to produce electricity from radioactive decay heat, have functioned for over 30 years (*6*, *7*). This high life time is due to the small thermal cycles (<20) inherent in space exploration and the design of the devices, which can sustain significant bowing stresses within the TE material (*7*). Vehicle exhaust gas temperatures, however, are above those usually associated with commercial TEGs and the number of thermal cycle severely exacerbates thermo-mechanical stress, sublimation, and interdiffusion, all of which need to be addressed for high

reliable TEGs waste heat regeneration (*8–11*). Nonetheless, if the same energy path shown in figure 2b is assumed to hold true for the M-1 Abrams Army vehicle, the driving range is predicted to increase 25 miles (*4*).

TE devices are typically comprised of n and p-type semiconductors connected together by a metal interconnect. As demonstrated by figure 3, these elements are placed thermally in parallel and electrically in series. Within the n-type element, the electrons are thermally excited by the high temperature and migrate to the low temperature. Within the p-type element, the holes also migrate from the high to low temperature regions causing current to flow, thus generating electricity directly from thermal energy.

Table 1. NASA missions, which use RTGs (*7*).

Mission	RTG	TE	Destination	Launch Year	Mission Length
Transit 4A	SNAP-3B7(1)	PbTe	Earth Orbit	1961	15
Transit 4B	SNAP-3B8 (1)	PbTe	Earth Orbit	1962	9
Apollo 12	SNAP-27 RTG (1)	PbTe	Lunar Surface	1969	8
Pioneer 10	SNAP-19 RTG (4)	PbTe	Outer Planets	1972	34
Triad-01-1X	SNAP-9A (1)	PbTe	Earth Orbit	1972	15
Pioneer 11	SNAP-19 RTG (4)	PbTe	Outer Planets	1973	35
Viking 1	SNAP-19 RTG (2)	PbTe	Mars Surface	1975	4
Viking 2	SNAP-19 RTG (2)	PbTe	Mars Surface	1975	6
LES 8	MHW-RTG (4)	Si-Ge	Earth Orbit	1976	15
LES 9	MHW-RTG (4)	Si-Ge	Earth Orbit	1976	15
Voyager 1	MHW-RTG (3)	Si-Ge	Outer Planets	1977	31
Voyager 2	MHW-RTG (3)	Si-Ge	Outer Planets	1977	31
Galileo	GPHS-RTG (2) RHU(120)	Si-Ge	Outer Planets	1989	14
Ulysses	GPHS-RTG (1)	Si-Ge	Outer Planets/Sun	1990	18
Cassini	GPHS-RTG (3) RHU(117)	Si-Ge	Outer Planets	1997	11
New Horizons	GPHS-RTG (1)	Si-Ge	Outer Planets	2005	3 (17)
MSL	MMRTG (1)	PbTe	Mars Surface	2011	3

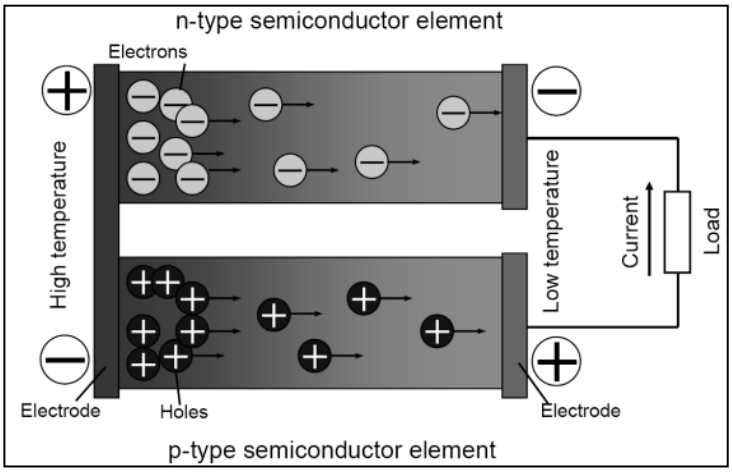

Figure 3. Underlying TEG mechanism (*26*, *19*)

A thermal resistance representation of a typical TEG module is displayed in figure 4. Within the exhaust pipe, temperatures can reach 1000 °C (*12*), depending on its engine proximity. To be converted into electrical energy, the heat contained in this exhaust must conduct through the exhaust pipe to the TE device through several layers, which hinder TE performance. The heat flow to the TEG can be improved through the use of fins within the pipe and by better managing the heat flow out of the device on the "cold-side," but at the cost of increased exhaust and coolant loop pressure drops. These issues mandate optimizing the entire automotive system to determine the best operating conditions (*12–14*).

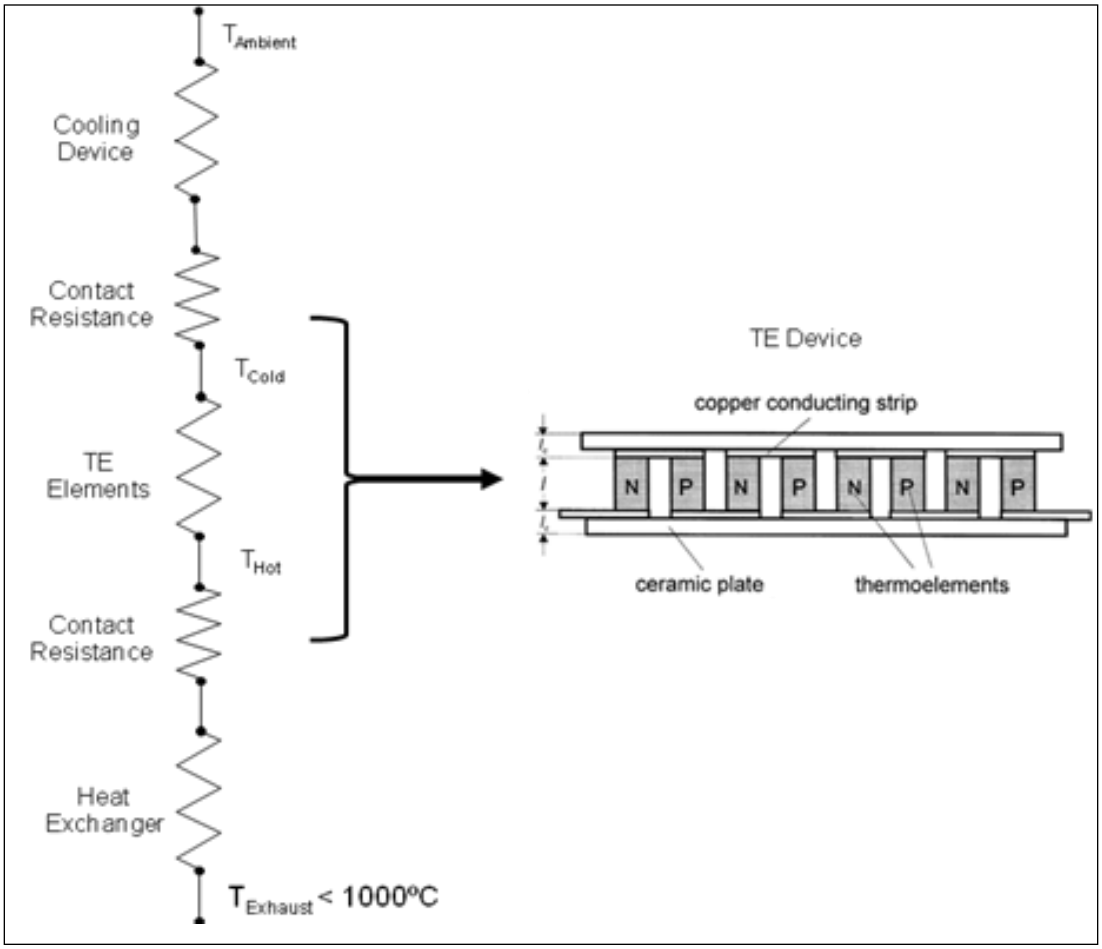

Figure 4. TEG thermal resistance representation (*16*).

The classical style of a TEG module is a flat (cylindrical geometries have also been studied [*15*]) array of TE devices, similar to that of figure 4, connected electrically in series to increase output power. This power depends on the temperature difference across the device, material properties, and contact resistances as shown in equation 1 (*16*):

$$P_{Out} = \frac{\alpha^2}{2\rho} \frac{NA(\Delta T)^2}{(l+n)(1+2r_c l_c/l)} \quad (1)$$

where α is the Seebeck coefficient ($\frac{\mu V}{K}$); ρ is the electrical resistivity (Ωm); A is the cross-sectional area of the TEs (m^2); N is the number of TE elements; ΔT is the hot (T_H) and cold side (T_C) temperature difference ($^\circ C$); l_c is the insulating ceramic layer thickness (m); n is the ratio of electrical contact resistivity to electrical resistivity; and r_c is the ratio of contact resistivity to thermal resistivity. The power is clearly limited to the inefficiencies of the TE material and is currently a major road block to wide TEG acceptance.

A TE material can be rated according to its efficiency of transforming thermal energy to electrical energy. This is typically defined as "the thermoelectric figure of merit" (Z), shown in equation 2:

$$Z = \frac{\alpha^2 \sigma}{k} \tag{2}$$

where k is the thermal conductivity ($\frac{W}{mK}$). Z can be manipulated through several techniques that amplify inherent material properties and is at times multiplied by its operating temperature in Kelvin to provide its dimensionless counterpart ZT (*17*, *6*, *18*).

To add quantitative context to the dimensionless ZT, it has been compared to the more familiar Carnot efficiency (thermodynamic maximum heat pump efficiency) and that comparison is displayed in figure 5. Clearly, a ZT larger than 14 is needed to approach a 40% Carnot efficiency (*19*). Presently, all commercial applications for TEGs operate across a small ΔT (<250 °C) and most state-of-the-art TE materials are around a ZT of 1 producing a 5%–6% overall efficiency. This makes TEGs the premiere technology of choice since no competing technology operates at such a low ΔT. However, for automotive exhaust gas applications, where the ΔT is much larger, greater ZT values are being investigated to produce higher efficiencies.

This brief review covers basic TE material principles, their performance as it refers to the figure of merit, and the reliability concerns surrounding the high temperature application of automotive exhaust waste heat regeneration.

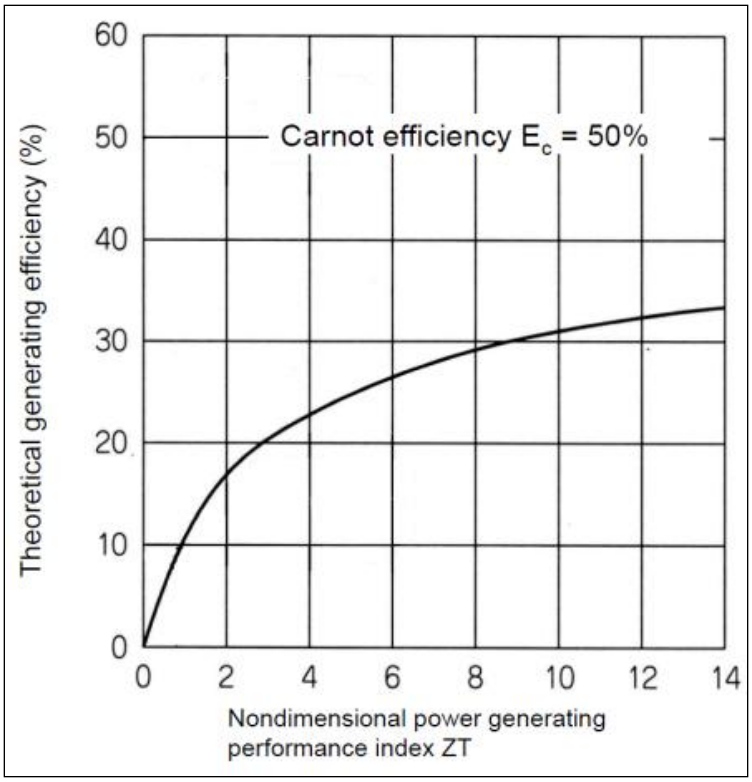

Figure 5. The Carnot efficiency as a function of the thermoelectric figure of merit (*19*).

2. Thermoelectric Material Principles

Much recent research in TE materials has been devoted to improving Z, which encompasses increasing the Seebeck coefficient and electrical conductivity while decreasing the thermal conductivity. This is difficult due to the immediate coupling of the properties, with the lattice conductivity being the least coupled (*20, 21*).

2.1 The Seebeck Coefficient

The Seebeck coefficient (α) is the coefficient of proportionality between the induced voltage difference and the temperature gradient across a material. Figure 6 shows two different materials (A and B) joined where a temperature gradient is held between the junction (T_1) and the materials' ends (T_2). This causes carriers to diffuse from the hot to cold junctions, ultimately creating a voltage difference proportional to the temperature gradient and the sum of the individual Seebeck coefficients ($\alpha_A \; and \; \alpha_B$), as shown in equation 3 (*1, 17*):

$$dV_{Seebeck} = \pm(a_A + a_B)dT \tag{3}$$

where $dV_{Seebeck}$ is the Seebeck voltage (μV). A general equation for the Seebeck coefficient of any individual semiconductor material is given in equation 4:

$$\alpha = \left(\frac{k}{e}\right)\left[ln\left(\frac{N_c}{n}\right) - \frac{3}{2}\right] \quad (4)$$

where N_C is the desity of states, n is the doping density cm^{-3}, k is the Boltzmann constant, and e is the electronic charge. Equation 4 can be modified for the case of carrier scattering common to metals or degenerate semiconductors (*20*), as given by equation 5:

$$\alpha = \frac{8\pi^2 k_B^2}{3eh^2} m^* T \left(\frac{\pi}{3n}\right)^{2/3} \quad (5)$$

where h is Planck's constant and m^* is the density of states effective mass. The Seebeck coefficient is proportional to temperature and inversly proportional to carrier concentration as shown explicitly in equation 5 and implicitly in equation 4 (*20*).

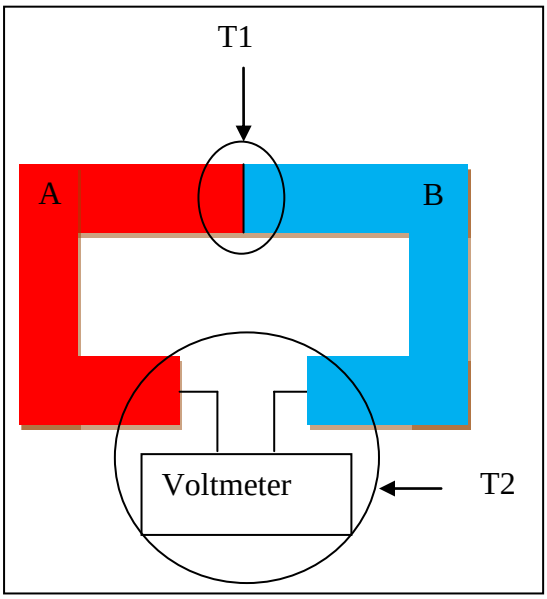

Figure 6. The Seebeck effect (*17*, *18*).

2.2 The Electrical Conductivity

The flow of current associated with the Seebeck voltage logically creates the search for TE materials with low parasitic Joule heating. Such materials possess high electrical conductivities that are directly proportional to the carrier concentration and mobility as given by equation 6 (*20*):

$$\sigma = ne\mu \quad (6)$$

where μ is the carrier mobility $\left(\frac{m^2}{Vs}\right)$. Coupling equation 2, 5, and 6 together, it is clear that an increase in carrier concentration will decrease the Seebeck coefficient, while increasing the electrical conductivity (*22*, *20*). These opposing effects have given rise to the development of the "Carrier Concentration Tuning Technique," where the $\alpha^2\sigma$ (black curve in figure 7a) of a material is maximized, as shown by figure 7a (*22*, *20*). The maximum depends heavily on the material system, but is often seen between 10^{19}cm^{-3} to 10^{21}cm^{-3} (*20*).

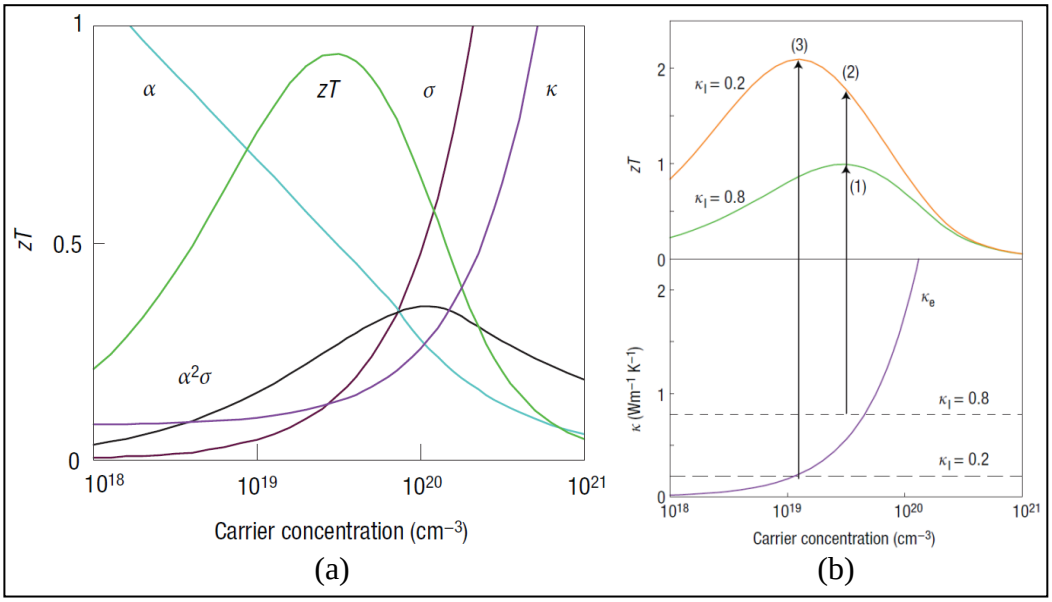

Figure 7. Carrier concentration tuning: (a) providing large *ZT* values and (b) changing the electrical thermal conductivity (*20*).

2.3 The Thermal Conductivity

As previously discussed, a reduced thermal conductivity is needed for TE materials to produce the highest figure of merit possible. This association is better understood through the division of the thermal conductivity into its sub-components, as shown by equation 7 (*20*):

$$k = k_e + k_l \tag{7}$$

where k_e is the contribution from free-carriers (electrons, holes) and k_l is the contribution from phonon (lattice) transport (*20*). As described by the Wiedemann-Franz law and shown in figure 7b, k_e is proportional to carrier concentration as provided by equation 8 (*20*):

$$k_e = ne\mu LT \tag{8}$$

where the Lorentz factor L is approximately $2.4\ X\ 10^{-8}\frac{J^2}{K^2C^2}$. Thus, the influence of carrier concentration on the electrical thermal conductivity requires the "Carrier Concentration Tuning Technique" to account for the thermal conductivity as well.

The lattice thermal conductivity can be decreased through site substitution, or alloying, with isoelectronic elements (*20*). These larger elements disrupt phonon transport without hindering the crystalline structure responsible for good electron conductivity. Complex crystal structures separating the electron-crystal from the phonon-glass and nanostructuring materials also reduce the lattice thermal conductivity (*20*).

3. Thermoelectric Material Performance

TE material research is mainly focused on increasing *ZT* by either using the "Carrier Concentration Tuning Technique" or reducing the lattice thermal conductivity. Both of these techniques are needed to achieve the largest possible Z within the automotive exhaust temperature domain shown in figure 8 (*6*). The temperature is usually within 600–800 °C, but may reach levels as high as 1000 °C (*12*).

The most common state-of-the-art commercial materials used are alloys based on $(Bi,Sb)_2(Se,Te)_3$ since they have the largest *ZT* for n and p-type materials up to 250 °C, as shown in figure 9a and b (*22*). This maximum *ZT* and the temperature at which it occurs can be modified through carrier concentration tuning, as shown in figure 9c. Conventional high temperature (500–900 K) TEGs, which are suitable for automotive waste heat regeneration, can use lead telluride (PbTe), $(GeTe)_{0.85}(AgSbTe2)_{0.15}$ (TAGS), or skutterudites with maximum *ZT* values around 0.8 (*20*). Conventional extreme-temperature (>900 K) TE materials typically comprise of silicon germanium (SiGe) for both n and p-type legs, with the latter containing relatively lower *ZT* values, as shown in figure 9a and b, respectively (*20*).

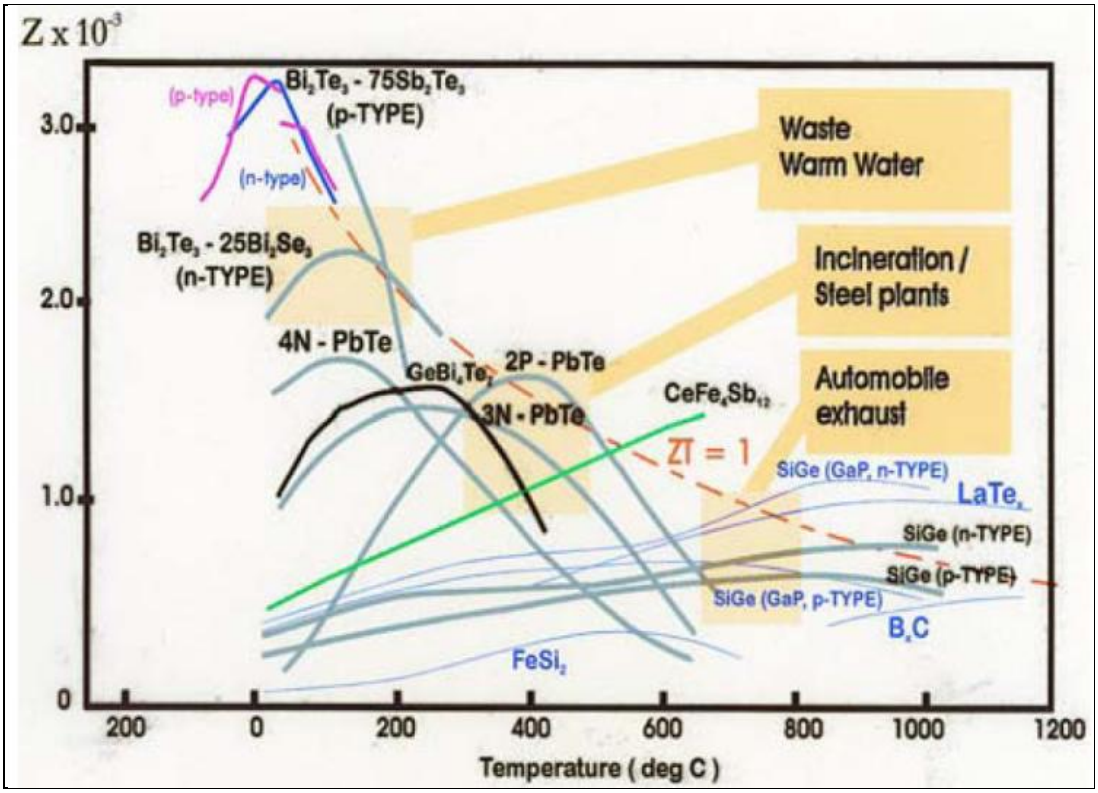

Figure 8. The TE figure of merit as a function of temperature with application-driven temperature ranges (*6*).

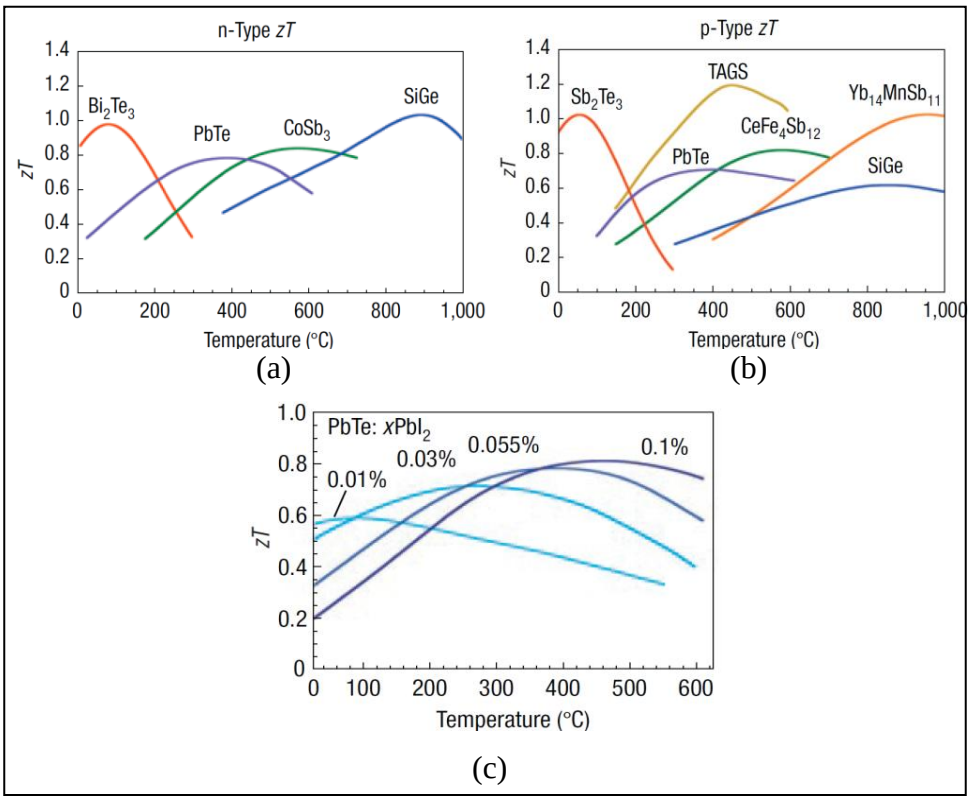

Figure 9. Figure of merit of (a) p-type, (b) n-type materials, and (c) doping concentration modifying the maximum *ZT* (*22*).

There are many methods of reducing the lattice thermal conductivity, of which only the most prominent were selected for this review. The first method scatters phonons by inserting large "rattling" structures into void spaces (*22*). These structures can be found in clathrates and skutterudites (*6*, *20*). A common skutterudite, cobalt triantimonide ($CoSb_3$), contains many covalent bonds, which require the filling of their octahedral voids (shown in figure 10a) with large rare-earth atoms to reduce their lattice conductivity (*20*). Ions can also be inserted to increase the needed disorder for low conductivity. With these discussed enhancements, skutterudites are known to produce *ZT* values of around 1 at temperatures of around 900 K, as shown in figure 10b.

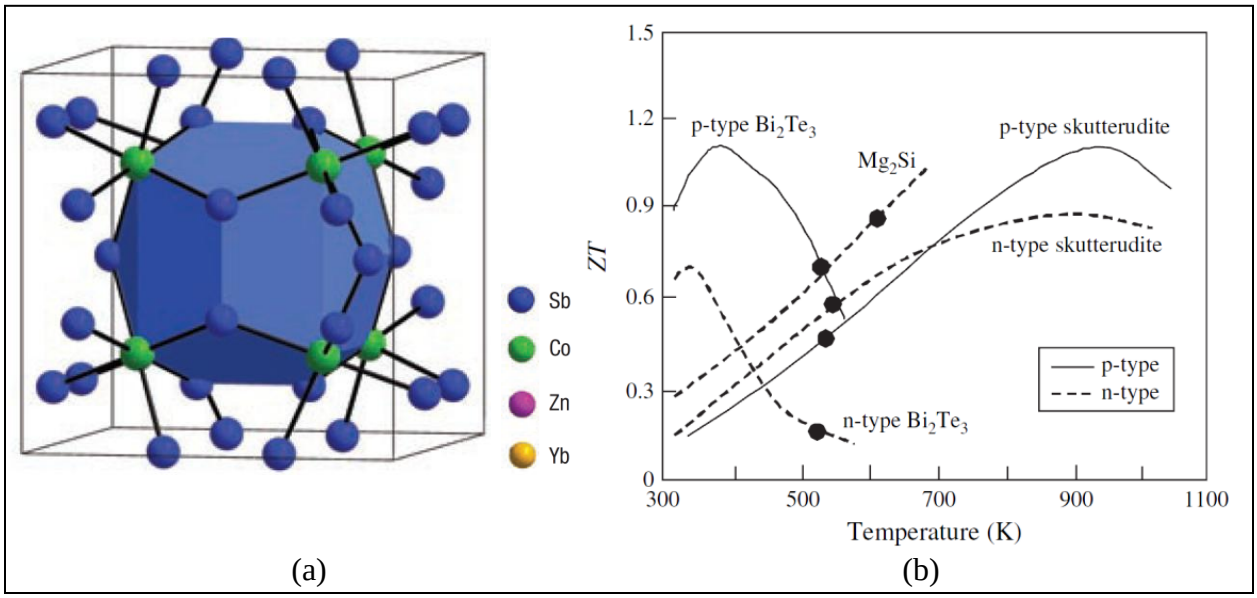

Figure 10. (a) Skutterdite structure of $CoSb_3$ with large blue void (*20*) and (b) the figure of merit for skutterudite materials (*1*).

Another method of reducing the lattice thermal conductivity is through the separation of the phonon-glass from the electronic crystal by complex structuring (*22*). A good example of this is the ytterbium manganese antimonide ($Yb_{14}MnSb_{11}$) Zintl compound, which is receiving attention from NASA to replace their current SiGe TE materials (*22*). These contain a valence-balanced combination of ionic and covalent bonds with the former donating electrons to the covalent bonds and the latter allowing high electron mobility (*20*, *23*). As shown in figure 11, this complex structure produces very low thermal conductivity resulting in *ZT* values greater than 1 at 900 °C (*20*).

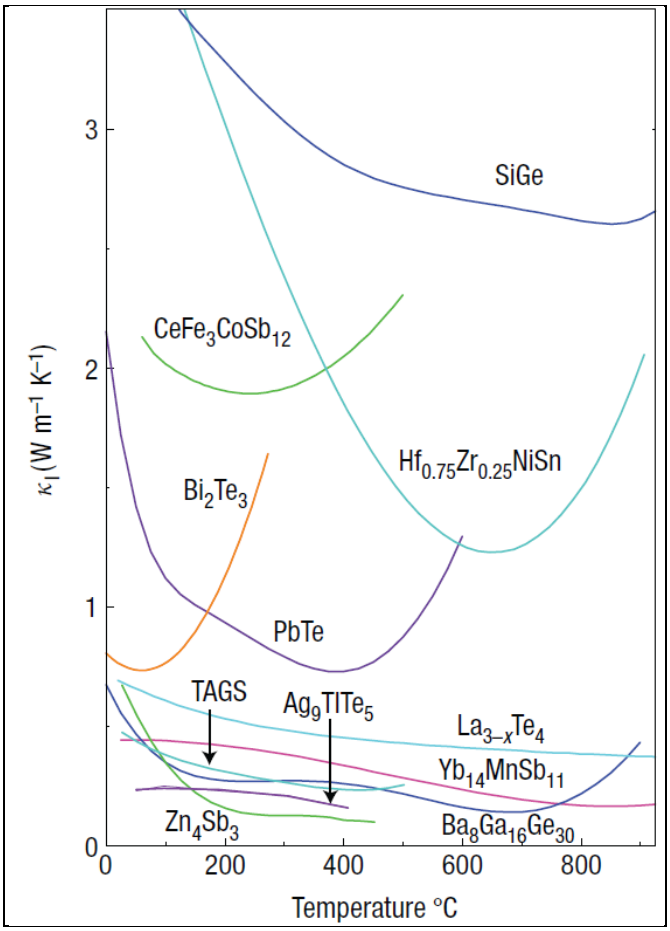

Figure 11. Thermal conductivity as a function of temperature for complex structures (*20*).

Another approach to achieve high *ZT* is the substructure approach, where different regions of the structure are imagined to enhance or retard the pertinent TE properties of electrical conductivity and thermal conductivity. Disordered structures produce low thermal conductivity where nanostructuring at the sub-nanometer scale increases the electrical conductivity through the use of quantum wells and dots (*22*). Currently, more research is needed to improve the *ZT* of these materials beyond 1, as shown in figure 12. However it is expected that the substructure approach coupled with multi-level phonon scattering methods (including nanostructuring) will provide the high Seebeck and electrical conductivity while retarding the thermal conductivity (*22*).

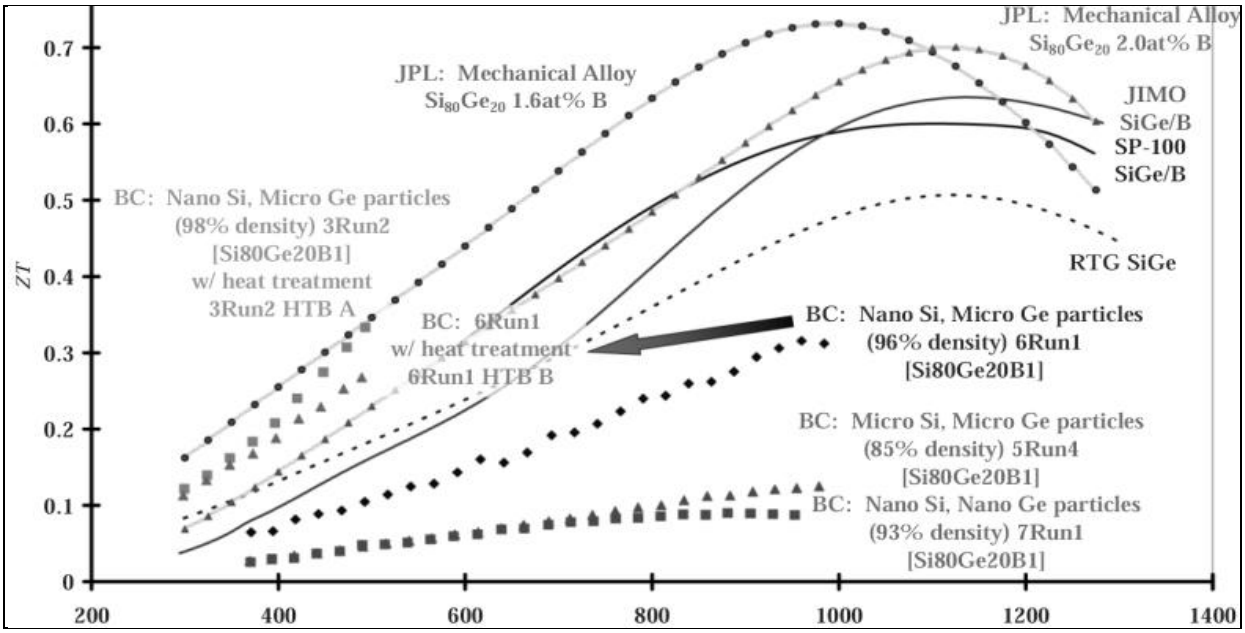

Figure 12. Figure merit for substructure (and nanostructured) materials (*29*).

4. Thermoelectric Generator Reliability

The main reliability concerns of TEGs are the induced thermo-mechanical stresses from coefficient of thermal expansion (CTE) mismatches, intermetallic growth between the structure layers, and TE material sublimation. These failure mechanisms are worsened by the high temperatures that occur within an automotive exhaust stream (<1000 °C [*12*]) as well as the high number of temperature cycles that readily occur due to changes in load and environment.

TEGs require large temperature differences ($T_{Hot} - T_{Cold}$) across the material junctions to generate significant power. This temperature difference causes significant bowing of the materials, as shown in figure 13 (*7*), due to the CTE mismatch of the TE materials, their metal interconnect, and their adjoining ceramic substrates (*11*). The CTE values for some high temperature TE materials are shown in table 2 (*11*). The CTE differences between structure layers ($\Delta\alpha \; in \; ppm/K$) subsequently causing interlayer stress (σ) along with the temperature difference ($\Delta T \; in \; K$) and the layer thicknesses as approximated by equation 9 (*11*):

$$\sigma = \frac{1+v_c}{1+v_c^2} \, E_c \Delta\alpha \Delta T \tag{9}$$

where E_c is the elastic modulus (Pa).

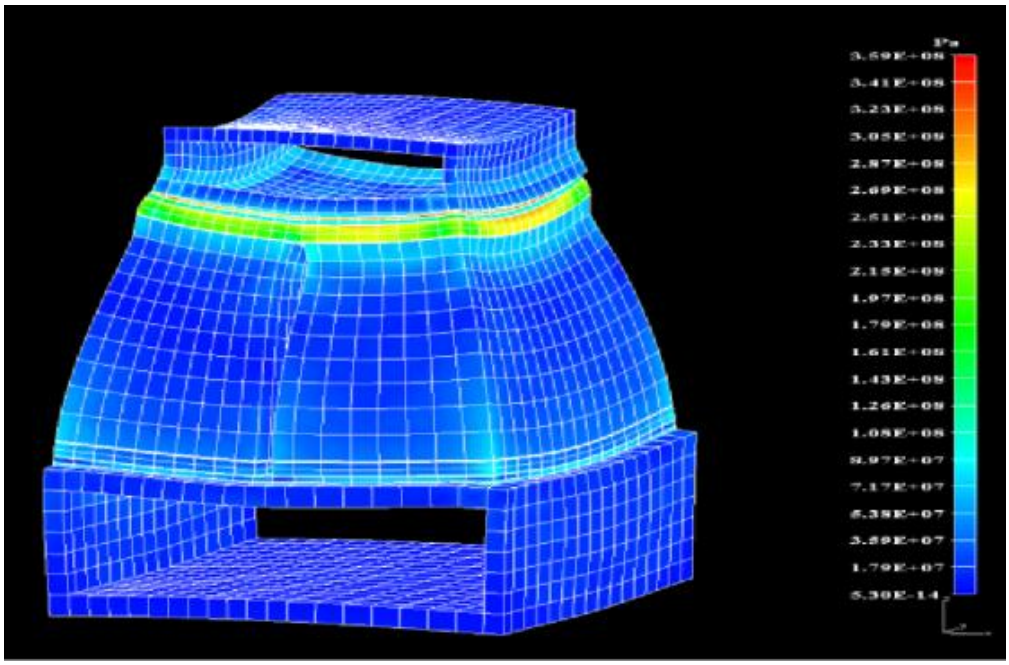

Figure 13. Deformation and stresses associated with large ΔT (*7*).

Table 2. Mean CTE values for high temperature TE materials (*11*).

Thermoelectric Material	CTE: Third Heating Cycle (ppm/K)[b]
p-nanostructured SiGe	~4.4 (323 K to 1273 K)
n-nanostructured SiGe	~4.1 (323 K to 1273 K)
n-mechanically alloyed SiGe	~5.8 (323 K to 1273 K)
p-$Yb_{14}MnSb_{11}$	~17.5 (323 K to 1273 K)
n-$CoSb_3$	~12.2 (473 K to 873 K)
p-$CeFe_3RuSb_{12}$	~14.5 (473 K to 873 K)

The evolution and growth of intermetallics between juxtaposed materials is another main failure mechanism. This failure is apparent when accelerated thermal tests are performed at constant elevated temperatures following the procedure outlined in reference 24 for $(Bi,Sb)_2(Se,Te)_3$. As is evident in figure 14, device failures increase suddenly at around 100 h, regardless of the temperature, pointing towards a common failure mechanism (*24*). Due to the high activation energy (0.85 eV) of intermetallic formation at the TE material and metallization interface, interdiffusion and chemical reaction between the TE material and its metal contact is believed to be a key failure mechanism. The continued growth of these brittle intermetallics leads to Kirkendall voiding causing the eventual increases in the electrical resistance (*24*). Contact migration and galvanic corrosion due to dissimilar materials at different electrochemical potentials are considered related failure mechanisms (*24*).

Intermetallic growth between $(Bi,Sb)_2(Se,Te)_3$ and the metallization can be remediated through the electroless deposition of nickel (Ni) layers (*25*). This layer provides a good contact by having low contact resistance, high mechanical strength, and diffusion protection, provided the Ni is sufficiently thick. (*25*). The characteristics have been subsequently studied as a function of Ni thickness at a constant temperature (135 °C) and the normalized thermal results are shown in figure 15 (*25*). For Ni thicknesses under 3 μm, 20%–25% increases in electrical resistance are seen in the first 500–600 h, producing only a 10% decrease in the figure of merit (*25*). This demonstrates that electrical resistance is a viable prognostic tool to predict intermetallic growth related failures.

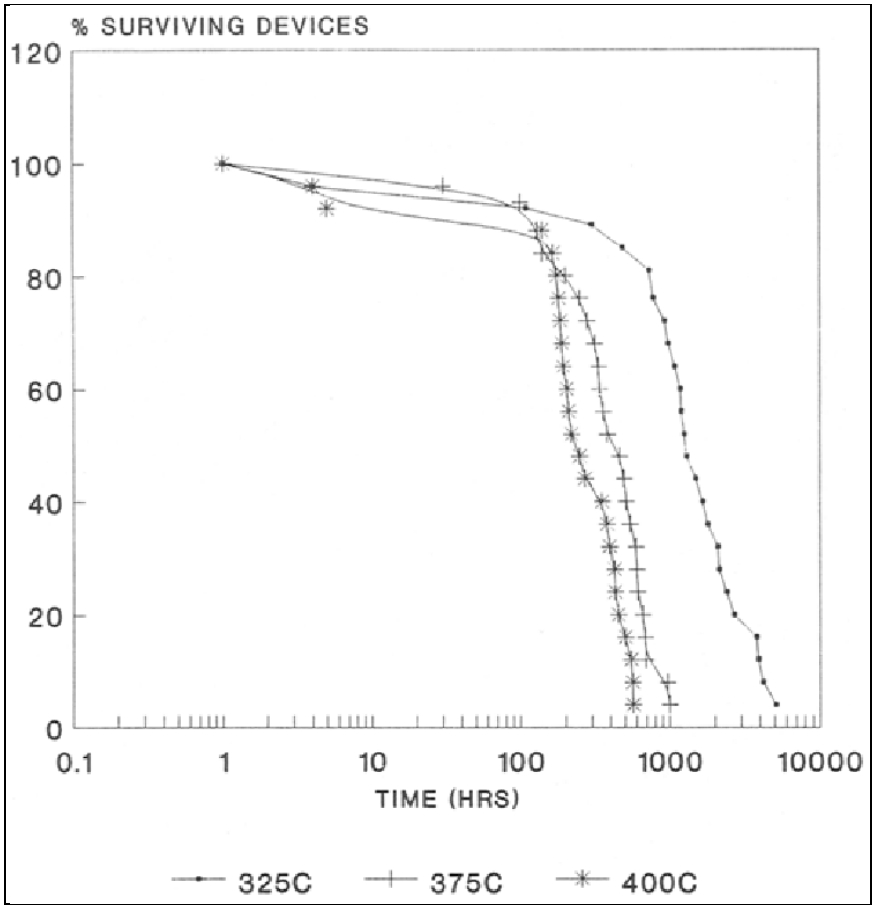

Figure 14. Percentage of survived $(Bi,Sb)_2(Se,Te)_3$ devices as a function of time and temperature (*24*).

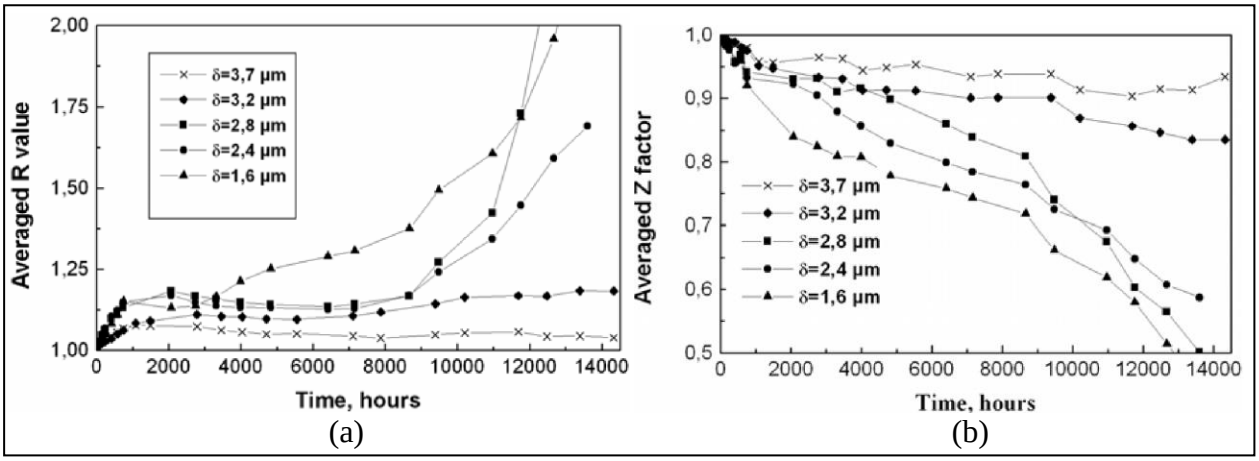

Figure 15. (a) Normalized electrical resistance as a function of time and (b) normalized Z as a function of time (*25*).

Due to the higher operating temperature of skutterudites allowing greater automotive waste heat regenerative applications, intermetallic growth of these materials have also been studied using accelerated tests at constant elevated temperatures (*9, 10*). In these studies, titanium (Ti) is used as a diffusion barrier between the TE $CoSb_3$ and molybdenum-copper (Mo-Cu) metallization (*9, 10*). As shown in figure 16 and equation 10, intermetallic layer thickness is proportional to the time the device is held at an elevated temperature as well as the temperature (*9, 10*).

$$Y = Y_o + \left(tD_o e^{\frac{-Q}{RT}}\right)^{0.5} \tag{10}$$

where Y is the intermetallic thickness at time t (m); Y is the initial intermetallic thickness at time t_o (m), t is the reaction time (s), D_o is the growth constant ($\frac{m}{s}$), Q is the activation energy ($\frac{KJ}{mol}$), and R is $8.314\,\frac{KJ}{mol}$.

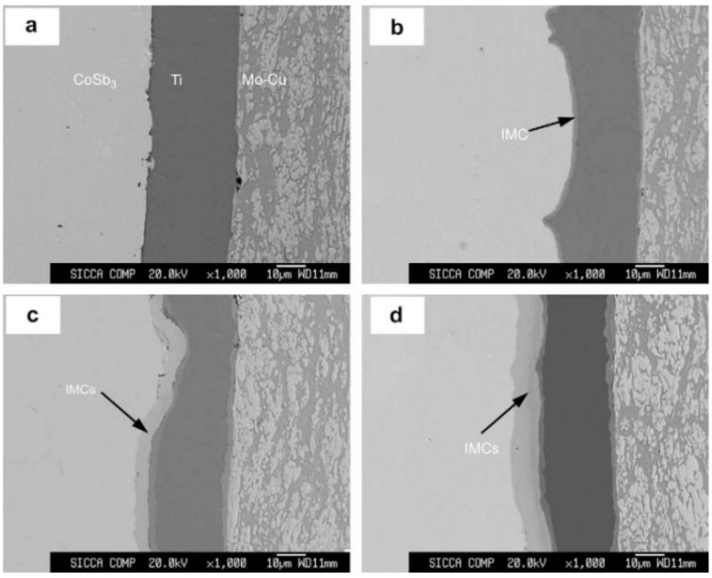

Figure 16. Scanning electron microscopy (SEM) micrographs of $CoSb_3$/Mo-Cu interfaces aged at 550 °C for: (a) 0, (b) 4, (c) 8, and (d) 20 days (*10*).

As with $(Bi,Sb)_2(Se,Te)_3$, the intermetallic growth causes the diffusion of molecules needed for high electrical conductivity away from the TE material, and thus, decreases electrical conductivity. These intermetallics are also quite brittle, causing crack formation and propagation within them, and as shown in figure 17, ultimately reduce the shear strength of the $CoSb_3$/ Mo-Cu.

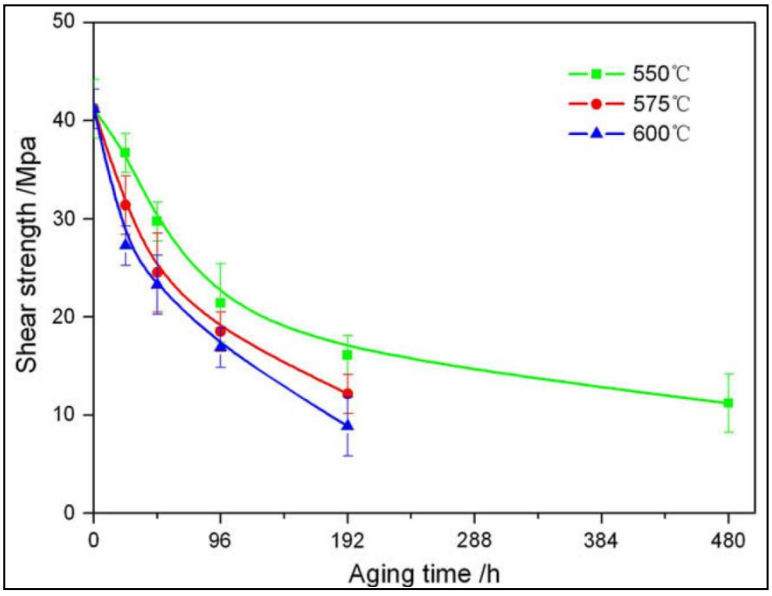

Figure 17. Shear strength of $CoSb_3$/Mo-Cu interface as a function of aging time and temperature (*10*).

The preferential sublimation of the antimony within skutterudites is another failure mechanism responsible for the degradation of the TE figure of merit (*8*). Antimony vapor can accumulate underneath the metal contact surface as shown in figure 18a (*8*). This evolution closely follows a parabolic rate law, which is highly a function of temperature, as shown in equation 11 (*8*) and plotted against real data in figure 18b (*8*)

$$(\Delta m)^2 = tk_o e^{\frac{Q}{RT}} \tag{11}$$

where Δm is the weight loss per unit area ($\frac{g}{cm^2}$) and k_o is the rate constant ($\frac{g^2}{cm^4 s}$). This evaporation of antimony degrades electrical conductivity and Seebeck coefficients, ultimately causing the reduction of the figure of merit, as shown in figure 19 (*8*). Following the sublimation proportionality with temperature, the *ZT* also degrades at elevated aged temperatures, as shown in figure 19 (*8*).

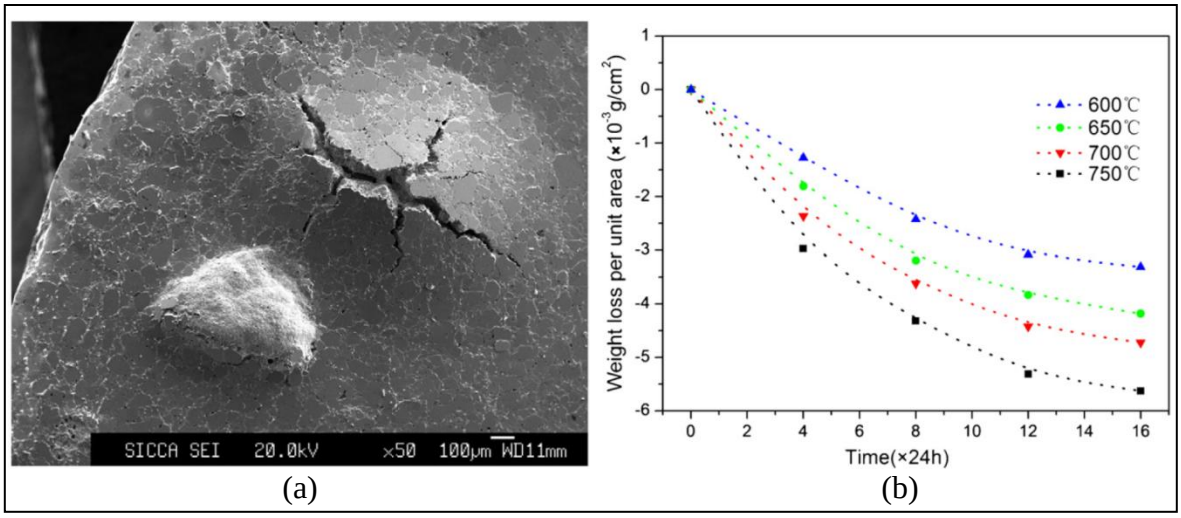

Figure 18. (a) $CoSb_3$ surface images after 750 °C thermal degradation test for 16 days and (b) mass loss as a function of time and temperature (*8*).

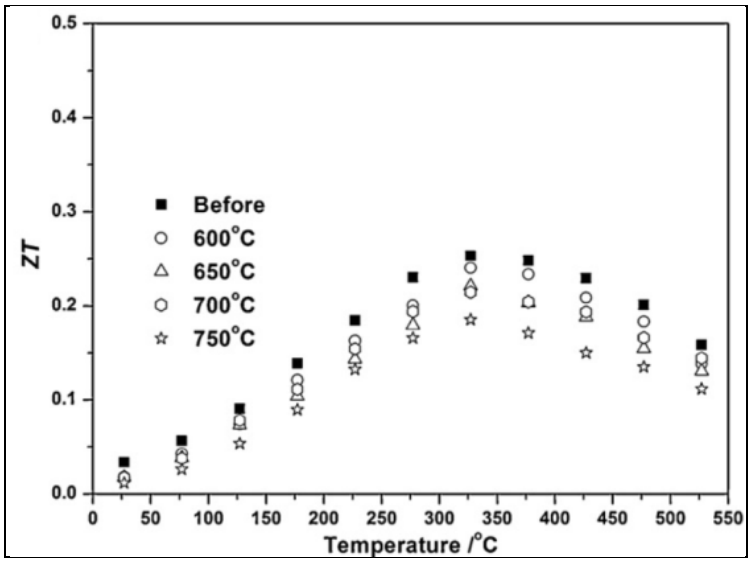

Figure 19. $CoSb_3$ figure of merit as a function of temperature and aged temperature with reductions due to sublimation (*8*).

Sublimation of TE devices is typically the mechanism that creates an upper temperature limit for TE materials. Some common TE materials and their associated sublimation temperature and rate constants are provided in table 3.

Table 3. TE material maximum temperature and associated sublimation rate constant (*7*).

Material	**Temperature**	**Rate Constant (k_o)**
PbTe	500 ºC	~9.4 x 10^{-2} g/cm^{2}h
n-Skutterdite	700 ºC	~2.15 x 10^{-2} g/cm^{2}h
p-Skutterdite	700 ºC	~2.7 x 10^{-2} g/cm^{2}h

5. Conclusion

TE waste heat generators on automobile exhaust pipes can have significant regenerative rates due to the amount and high temperature of the waste heat. While commercial modules based on $(Bi,Sb)_2(Se,Te)_3$ have efficiencies entirely consistent with small ΔTs, the larger ΔTs for automobile exhaust applications promise to more than double the efficiency! However, those larger ΔTs are too extreme for $(Bi,Sb)_2(Se,Te)_3$, so there is rich opportunity for TEG research. This research currently focuses on solutions that will allow commercial products to be produced with long-lifetime and large conversion efficiencies. This brief review covers basic TE material principles and performance of popular TE materials like $(Bi,Sb)_2(Se,Te)_3$, $CoSb_3$-based skutterudites, and $Yb_{14}MnSb_{11}$ Zintls. The reliability concerns surrounding thermo-mechanical stress associated with CTE mismatch, intermetallic formation, and sublimation are also briefly discussed.

6. References

1. Funahashi, R.. Waste Heat Recovery Using Thermoelectric Oxide Materials. *Science of Advanced Materials* **2011**, *321* (1457), 682–686.
2. International World Energy, *Wold Energy Outlook 2006 Edition*, International World Energy, 2001.
3. Board, D. S. Report of the Defense Science Board Task Force on DoD Energy Strategy, *More Fight-Less Fuel*, Office of the Under Secretary of Defense for Acquisition, Technology, and Logistics, Washington, D.C., 2008.
4. Taylor, P. Thermoelectric Materials, Measurements, and Opportunities for Energy Harvesting. in *Materials, Preparation,and Characterization in Thermoelectrics*, Boca Raton, Florida, Taylor & Francis Group, 2012, pp. 20–1.
5. Eady, S.S.R.B.a.S.D.D. Sustain the Mission Project: Casualty Factors for Fuel and Water Resupply Convoys; Final Technical Report; Army Environmental Policy Institute, Arlington, Virginia, 2009.
6. Rowe, D. Thermoelectric Easte Heat Recovery as a Renewable Energy Source. *International Journal of Innovations in Energy Systems and Power* **2006**, *1* (1), 13–23.
7. Fleurial, J.-P.; Caillat, T.; Nesmith, B.; Ewell, R.; Carr, D.W.G.; Jones, L. Thermoelectrics: From Space Power Systems to Terrestrial Waste Heat Recovery Appications. in *2011 Thermoelectrics Applications Workshop*, San Diego, 2011.
8. Zhao, D.; Tiana, C.; Liua, Y.; Zhana, C.; Chenb, L. High Temperature Sublimation Behavior of Antimony in CoSb3 Thermoelectric. *Journal of Alloys and Compounds* **2011**, *509* (6), 3166–3171.
9. Zhao, D.; Tiana, C.; Liua, Y.; Zhana, C.; Chen, L. Interfacial Evolution Behavior and Reliability Evaluation of CoSb3/Ti/Mo–Cu. *Journal of Alloys and Compounds* **2009**, *477* (1–2) 425–431.
10. Zhao, D.; Xiaoya Li, He, L.; Jiang, W.; Chen, L. High Temperature Reliability Evaluation of CoSb3/Electrode Thermoelectric Joints. *Intermetallics* **2009**, *17* (3), 136–141.
11. Ravi, V.; Firdosy, S.; Caillat, T. Thermal Expansion Studies of Selected High-Temperature. *Journal of Electronic Materials* **2009**, *38* (7), 1433–1442.
12. Vazquez, J.; Sanz-Bobi, M.; Palacios, R.; Arenas, A. Automobiles, State of the Art Thermoelectric Generators Based on Heat Recoverd from Exhaust Gases of 2002.

13. Serksnis, A. Thermoelectric Generator for Automotive Charging System. in *11th Intersociety Conversion Engineering Conference*, New York, 1976.

14. Freeman, A. Master's Thesis: A Thermoelectric Generation Subsystem Model for eat Recovery Simulations, Rochester: Department of Mechanical Engineering, Rrochester Institute of Techonology Rochester, 2011.

15. Takanose, E.; Tamakoshi, H. The Development of Thermoelectric Generator for Passenger Car. in *12th International Conference on Thermoelectircs*, Yokohama, Japan, 1993.

16. Rowe, D. M.; Mn, G. Evaluation of Thermoelectric Modules For Power Generation. *Journal of Power Sources* **1998**, *73* (2), 193–198.

17. Allan, A.B.-C.; Kraus, D. Thermoelectric Coolers. in *Thermal Analysis and Control of Electronic Equipment*, New York, Hemisphere Publishing Corporation, 1983, pp. 435–465.

18. Nochetto, H. Hotspot Remediation Using Germanium Self Cooling Technology (Thesis), College Park: University of Maryland, 2011.

19. Kawamotok, H. R&D Trends in High Efficiency Thermoelectric Conversion Materials for Waste Heat Recovery. Science and Technology Trends, 2009.

20. Snyder, G. J.; Toberer, E. S. Complex Thermoelectric Materials. *Nature Materials* **2008**, *7*, 105–114.

21. Zevalkink, A.; Toberer, E.; Zeier, W.; Flage-Larsen, E.; Snyder, J. Ca3AlSb3: An Inexpensive, Non-toxic Thermoelectric Material for Waste Heat Recovery. *Energy and Environmental Science* **2010**, *4*, 510–518.

22. Snyder, G. J. Electronic Strategies for high Thermoelectric ZT in Bulk Materials. in *High Temperature Thermoelectric Confrence*, 2009.

23. Kauzlarich, S.R.B.S.M.; Gascoin, F.; Snyder, G. J. Yb14MnSb11: New High Efficiency Thermoelectric Material for Power Generation. *Chemistry of Materials* **2006**, *18* (7), 1873–1877.

24. Kiely, J. H.; Morgan, D. V.; Rowe, D. Failure Analysis of a Thin Film Thermoelectric Generator. in *The 13th International Conference on Thermoelectrics*, Kansas City, Missouri, 1995.

25. Semenyuk, V.; Antonenko, A. Diffusion Protection of Thermoelectric Cooler Junctions as a Means of Increasing its Reliability. in *5th European Conference on Thermoelectrics*, Odessa, Ukraine, 2007.

26. Shindo, T.; Nakatani, Y; Oishi, T. Thermoelectric Generating System for Effective Use of Unutilized Energy. *Toshiba Review* **2008**, *63* (2), 7–10.

27. Yang, J. Potential Applications of Thermoelectric Waste Heat Recovery in the Automotive Industry. in *24th Internation Conference on Thermoelectrics*, Clemson, 2005.

28. Stabler, F. Automotive Applications of High Efficiency Thermoelectrics. in *DARPA/ONR Program Review and DOE High Efficiency Thermoelectric Workshop*, San Diego, 2002.

29. Dresselhaus, M.; Chen, G.; Tang, M.; Yang, R.; Lee, H.; Wang, D.; Ren, Z.; Fleurial, J.-P.; Gogna, P. New Directions for Low-Dimensional Thermoelectric Materials. Advanced Materials **2007**, *19*, 1043–1053.

30. Cusack, N.; Kendall, P. The Absolute Scale of Thermoelectric Power at High Temperature. 7 July 1958. http://iopscience.iop.org/0370-1328/72/5/429 (accessed 3 March 2012).

31. Clack, G. A. *CRC Handbook of Thermoelectrics*, Boca Raton, FL: CRC Press, 1995.

List of Symbols, Abbreviations, and Acronyms

CO_2	carbon dioxide
$CoSb_3$	cobalt triantimonide
CTE	coefficient of thermal expansion
DoD	Department of Defense
Moo-Cu	molybdenum-copper
NASA	National Aeronautics and Space Administration
Ni	nickel
PbTe	lead telluride
RTGs	radioisotope thermoelectric generators
SEM	scanning electron microscopy
SiGe	silicon germanium
TAGS	$(GeTe)_{0.85}(AgSbTe2)_{0.15}$
TE	thermoelectric
TEGs	thermoelectric generators
Ti	titanium
$Yb_{14}MnSb_{11}$	ytterbium manganese antimonide

1 (PDF only) DEFENSE TECHNICAL INFORMATION CTR
DTIC OCA
8725 JOHN J KINGMAN RD
STE 0944
FORT BELVOIR VA 22060-6218

1 DIRECTOR
US ARMY RESEARCH LAB
IMAL HRA
2800 POWDER MILL RD
ADELPHI MD 20783-1197

1 DIRECTOR
US ARMY RESEARCH LAB
RDRL CIO LL
2800 POWDER MILL RD
ADELPHI MD 20783-1197

7 US ARMY RSRCH LAB
ATTN RDRL SED E SHAFFER
ATTN RDRL SED E L BOTELER
ATTN RDRL SED E H NOCHETTO
ATTN RDRL SED E P BARNES
ATTN RDRL SED E A LELIS
ATTN RDRL SEE I P TAYLOR
ATTN RDRL SEE I J MADDUX
2800 POWDER MILL RD
ADELPHI MD 20783-1197